Food Control 179 (2026) 111575

Contents lists available at ScienceDirect

Food Control

journal homepage: www.elsevier.com/locate/foodcont

Intelligent thermography for detecting melamine adulteration in powdered milk

Alicia Ortiz-Chiliquinga [a], Ana M. Pérez-Calabuig [a], Sandra Pradana-López [a], John C. Cancilla [b], José S. Torrecilla [a,c,*]

[a] Departamento de Ingeniería Química y de Materiales, Universidad Complutense de Madrid, 28040, Madrid, Spain
[b] Allele Biotechnology, 6404 Nancy Ridge Dr., San Diego, CA 92121, USA
[c] Escuela Politécnica Superior del Ejercito, 28002, Madrid, Spain

ARTICLE INFO

Keywords:
Adulteration
Milk powder
Melamine
Thermography
Convolutional neural networks
ResNet34

ABSTRACT

A non-destructive, fast, inexpensive, and accurate technique was developed to detect and semiquantify melamine in powdered milk using a combination of infrared thermography and convolutional neural networks, specifically the ResNet34 architecture. Three types of powdered milk were mixed with varying melamine concentrations (0.5–10 ppm), each prepared in triplicate to ensure reproducibility. After heating, nearly 28,500 thermographic images were collected during the cooling process. Ninety percent of the dataset was used for training and internal validation of the convolutional neural networks, while the remaining 10 % was reserved for blind testing. The resulting algorithm classified thermographic images by milk type and melamine concentration with an overall accuracy exceeding 98 %. This performance highlights the potential of the proposed method as a reliable tool for detecting food fraud and ensuring dairy product quality, with an empirical detection limit of 0.5 ppm, well below the regulatory threshold for infant milk formulas.

1. Introduction

Food adulteration is a common fraudulent practice that threatens public health and undermines the credibility of the food industry (Spink & Moyer, 2011). In milk and milk-derived products, adulterants such as water, starch, detergents, and melamine are frequently detected. Melamine, a triazine compound with high nitrogen content (66 % by mass), has been widely used to falsely elevate protein levels in the Kjeldahl nitrogen test (Yan, 2012). Despite its low acute oral toxicity, chronic exposure has been linked to kidney damage, particularly in infants (Guo et al., 2014; Sánchez-Martín et al., 2018). Following the 2008 melamine crisis in China, which led to severe health consequences for over 200, 000 children (Lam et al., 2008), the European Commission set maximum melamine limits of 2.5 mg/kg for general foods and 1.0 mg/kg for powdered infant formulas (European Union, 2008).

Analytical methods commonly used for melamine detection include high-performance liquid chromatography (HPLC) with mass spectrometry, Raman spectroscopy, immunoassays like ELISA, and biosensors (Guo et al., 2014; Liu et al., 2012; Tittlemier, 2010). While highly sensitive, these techniques are often expensive, require specialized personnel, and are unsuitable for real-time or on-site analysis (Xie et al., 2015). In response, portable alternatives using Raman spectroscopy and electrochemical sensors have emerged (Liu & Xu, 2023; Shalileh et al., 2023a, Shalileh et al., 2023b; Yang et al., 2023), but these too present limitations such as complex calibration, chemometric modeling, and the need for special reagents or electrodes. Photoacoustic spectroscopy also shows promise but remains in development (Wu et al., 2023).

Infrared thermography (TIR) has gained interest as a non-destructive, fast, and portable method for food inspection (Guo et al., 2014; Gowen et al., 2010; Huerta-Herraiz et al., 2019). It measures surface temperature patterns that may vary with sample composition and structure. Because melamine alters the thermal conductivity and heat retention of milk powders (Feng et al., 2012; Finete et al., 2013), its presence can subtly change the cooling pattern of samples. While these differences are imperceptible to the human eye, they can be captured by thermographic imaging and identified by convolutional neural networks (CNNs), which excel in image classification tasks (Soffer et al., 2019; Yamashita et al., 2018; Ranjbar et al., 2020).

* Corresponding author. Departamento de Ingeniería Química y de Materiales, Universidad Complutense de Madrid, 28040, Madrid, Spain.
E-mail addresses: aliciaor@ucm.es (A. Ortiz-Chiliquinga), anampe08@ucm.es (A.M. Pérez-Calabuig), spradana@ucm.es (S. Pradana-López), jcancilla@allelebiotech.com (J.C. Cancilla), jstorre@ucm.es (J.S. Torrecilla).

https://doi.org/10.1016/j.foodcont.2025.111575
Received 2 May 2025; Received in revised form 8 July 2025; Accepted 15 July 2025
Available online 17 July 2025

CNNs have already demonstrated success in detecting food fraud, including in honey, olive oil, rice, and coffee (Izquierdo, Lastra-Mejías, González-Flores, Cancilla, et al., 2020a, Izquierdo, Lastra-Mejías, González-Flores, Cancilla, et al., 2020; Estrada-Pérez et al., 2021; Pradana-López et al., 2021). Beyond food analysis, CNNs have been used in medical imaging for tasks such as cancer or thyroid nodule detection (Ting et al., 2019; Zhou et al., 2020). In this context, this study proposes a novel combination of infrared thermography and ResNet34-based CNNs for melamine detection in powdered milk, aiming to offer a practical, accurate, and low-cost tool for food fraud detection and quality control, particularly in field-based or resource-limited settings.

2. Materials and methods

This section describes the milk powder samples analyzed, the materials and equipment used, and the mathematical model employed to process the results.

2.1. Types of milk and sample preparation

In this study, three types of powdered milk were used: whole milk (Brand: Asturiana, Expiry date: March 15, 2023), skim milk recommended for infants older than six months (Brand: Nestlé, Expiry date: March 15, 2023), and skim milk for infants younger than one month (Brand: Nestlé Sveltesse, Expiry date: June 15, 2023). All the products were purchased in a supermarket in Madrid (Spain) and were used within the expiration date. Melamine 99 % (Alfa Aesar; CAS 108-78-1) was used as the adulterant in the study.

A total of 31 samples were prepared: 27 adulterated and four pure, which included the three types of powdered milk and melamine. Each concentration level was prepared in triplicate for each milk type, resulting in three physically independent samples per concentration. This replication strategy ensures that the observed thermal differences are representative and not due to random variation. For each physical sample, multiple regions of the surface were imaged, and thousands of frames were captured during the cooling process. This approach increased both the variability and robustness of the dataset used for model training and validation. The range of concentrations was established between 0.5 and 10 ppm of melamine (0.0, 0.5, 1.0, 2.0, 2.5, 3.0, 4.0, 5.0, 7.5, and 10.0), which also covers concentrations lower than those legally accepted in powdered milk, both for adults (2.5 ppm) and for infants (1 ppm) (European Union, 2008)

2.2. Thermographic imaging

The adulterations were detected by training a mathematical model to distinguish thermographic images depending on the adulteration state of the milk samples imaged. In this work, an Optris PI model 450 thermographic camera (Optris GmbH, Berlin, Germany) was used, which uses infrared sensors to detect long-wave infrared emissions, which are then correlated with the surface temperature of the objects recorded (Huerta-Herraiz et al., 2019). Active thermography was employed in this study, with samples initially heated and thermographic images subsequently recorded during the cooling phase. In order to capture all possible thermal changes of each sample, since adulterations can originate differences in the thermographic profile, their cooling patterns were recorded using the described camera, obtaining videos in RAVI format. Subsequently, the frames of the different videos were extracted in TIFF format.

For accurate and consistent thermal imaging, the emission coefficient (emissivity) of the camera was set to 0.95, a standard value suitable for organic samples such as milk powder. The temperature measurement accuracy of the Optris PI 450 camera is $\pm 2\ ^{\circ}C$ or 2 % of the measured value, as specified by the manufacturer. To minimize potential environmental influences on cooling curves, experiments were conducted under controlled laboratory conditions with an ambient temperature of $24 \pm 1\ ^{\circ}C$ and relative humidity of 50 ± 5 %. These controls ensured the reproducibility and reliability of the thermal profiles captured.

The thermographic imaging setup consisted of an Optris PI 450 thermal camera (Optris GmbH, Berlin, Germany) mounted on a vertical support to allow precise focusing of the camera lens on the milk powder samples placed below. The camera was positioned at a fixed height above the samples, ensuring consistent distance and angle throughout the data collection process (Cancilla et al., 2022). The samples were carefully distributed in a thin, uniform layer on a flat cardboard surface to maintain a consistent thermal profile across all measurements. This arrangement minimized external interferences and allowed reliable acquisition of thermal images for subsequent analysis.

In order to ensure homogeneity of all the samples during recording, they were spread out on a sheet of paper in a uniform layer of at least 1 cm thickness, fully covering the entire sample holder. This ensured a stable background and avoided any interference from the paper substrate in the thermographic recordings. Subsequently, each sample was placed in an oven at 55 °C for 20 min, with a progressive heating rate of approximately 1.5 °C/min to ensure that all samples followed the same controlled process and reached the same final temperature, without chemically altering the melamine. This condition was chosen to guarantee that melamine detection using the thermographic methods employed was not compromised (Cancilla et al., 2022). After this time, the samples were removed from the oven, and the cooling process was recorded with the camera positioned perpendicularly until they reached room temperature (24 °C). We acknowledge that alternative heating conditions could be explored in future studies, provided they ensure the chemical integrity and detectability of melamine.

At this temperature (55 °C), melamine remains chemically stable and does not undergo decomposition or transformation into related compounds such as ammelide, ammeline, or cyanuric acid. These derivatives typically form under much higher thermal stress or in acidic hydrolytic conditions (Feng et al., 2012; Guo et al., 2014). Therefore, under the mild heating conditions used in this study, the melamine content is expected to remain unchanged, ensuring that the observed thermal profiles reflect physical rather than chemical transformations of the samples.

Additionally, the heating temperature of 55 °C is sufficiently low to avoid inducing physicochemical alterations in the milk powder matrix. Key components such as lactose, proteins (especially casein and whey proteins), and lipids remain structurally stable at this temperature. Protein denaturation in milk typically begins above 65–70 °C, depending on time and pH (Chandan & Kilara, 2011), while lipid oxidation and Maillard reactions are also negligible at 55 °C over short periods. Therefore, the selected heating conditions ensure that the thermal response captured by the camera reflects the inherent heat transfer characteristics of the samples rather than compositional degradation.

The videos were processed using the Optris PIX Connect thermography software package, developed specifically for the analysis of thermographic images. First, a cooling curve was constructed for each sample, plotting temperature (°C) versus time (s). Analysis of the curves revealed that the cooling profile of the samples varied as a function of melamine concentration.

This behavior can be explained by the thermal properties of melamine, which differ from those of the milk powder matrix. Melamine exhibits a relatively low specific heat capacity and distinctive thermal conductivity, which subtly influence the heat retention and transfer dynamics of the adulterated samples (Feng et al., 2012; Finete et al., 2013). The addition of melamine modifies the thermal inertia of the product, affecting how quickly it cools once removed from the heat source. Even small quantities can alter the surface temperature distribution and its dissipation rate, generating variations in the thermographic profile captured during the cooling process. These changes, while imperceptible to the human eye, can be detected through infrared imaging and effectively recognized by CNNs trained on large thermographic datasets.

In general, the temperature range where a sharp average temperature drop occurred was between 40.0 °C and 36.0 °C. Therefore, frames were extracted from the videos within this range, and to highlight the most significant thermal differences and their locations, the temperature scale was adjusted to span from 25.0 °C to 42.1 °C using a consistent color palette.

This temperature range (25.0–42.1 °C) was selected after preliminary analysis revealed that the most distinguishable cooling patterns associated with melamine concentration were concentrated in this interval. At higher temperatures (>42 °C), thermal gradients between samples were minimal and unstable due to rapid surface equilibration, limiting the detection of consistent thermal features. Conversely, at temperatures below 25 °C, the samples approached ambient temperature, resulting in low thermal contrast and increased image noise, which reduced the model's ability to extract relevant discriminatory information. Therefore, restricting the temperature window to 25.0–42.1 °C ensured the inclusion of the most informative and stable thermographic data for model training and validation.

Thus, a large database of thermal images was obtained, containing a total of 28,485 frames, which was used both for training and optimizing a CNN-based algorithm, and for blind validation, with the goal of detecting fraudulent mixtures of powdered milk.

2.3. Deep learning algorithms trained

The concept of deep learning refers to a set of multilayered neural network-based algorithms within the field of artificial intelligence (Bernabe et al., 2021). The complexity of the neural network depends on the number of layers and matrices forming each layer (Zhu et al., 2018). It is necessary to train the network with data (learning process) to lower the difference between the results it provides and the real outputs of the data points (Yamashita et al., 2018).

One of the main types of deep neural networks are CNNs, originally designed for image analysis, as they are able to highlight distinguishing features and derive them into more complex properties, enabling image classification (Soffer et al., 2019). These networks are able to learn from 3D (video), 2D (image), and 1D (text or audio) input data (Ranjbar et al., 2020).

The CNN topology comprises of an input layer, convolutional layers, pooling layers alternating with the convolutional ones, fully connected layers, and an output layer. The convolutional layers are responsible for extracting the most characteristic patterns from the image, while the pooling layers reduce the number of parameters and computational requirements in the network. The fully connected layers are responsible for mapping these patterns (Estrada-Pérez et al., 2021; Zhu et al., 2020). This structure allows shallower layers to recognize generic images by detecting small features, such as edges or textures, while deeper layers tend to be more specific in their recognition, as they detect more complex structures, such as shapes or partial objects, until reaching the final classification (Pradana-López et al., 2021).

The convolution operation is based on a matrix product (image × filter), in which the convolution filter (kernel) is superimposed on the input image and moved over it until all the pixels that form it have been traversed. Thus, a two-dimensional feature map, smaller than the input image, is generated (Izquierdo, Lastra-Mejías, González-Flores, Pradana-López, et al., 2020b). The distance between two filter positions in the convolution is called stride, one being its most common value (Izquierdo, Lastra-Mejías, González-Flores, Cancilla, et al., 2020a).

To maintain the dimensions of the input image after applying the convolution operation, the zero-padding technique is employed, which consists of adding zeros symmetrically to the input matrix. It is useful when the image dimensions must be preserved after the convolution operation is applied (Bernabe et al., 2021; Estrada-Pérez et al., 2021).

The feature map resulting from convolution requires the application of an activation function to establish the relationship of the matrices in the step between a convolutional layer and a pooling layer. In CNNs, the most commonly used activation function is the rectified linear unit (ReLU) function, $f(x) = \max(0, x)$, which accepts the input values of a neuron if it is positive, while returning 0 if the input is negative (Zhang et al., 2018).

After the large number of convolutional operations, the pooling layers carry out the subsampling process, which is to reduce the dimensions of the feature maps, i.e., the removal of irrelevant information. This is beneficial for the network, as it reduces computational load and overfitting problems (Izquierdo, Lastra-Mejías, González-Flores, Pradana-López, et al., 2020b; Ranjbar et al., 2020). The most frequent pooling method is Max Pooling, where the maximum value of the matrix is taken, due to the fact that it provides better network performance (Bernabe et al., 2021; Zhu et al., 2018).

Finally, the fully connected layers, also called classifier layers, are responsible for recognizing the features extracted in the previous layers (Torrecilla et al., 2007, 2008). For the final classification of an image, the softmax function is applied, which calculates the probability of belonging of each of the images to a certain class (Estrada-Pérez et al., 2021; Pradana-López et al., 2022). The network was trained to perform multiclass classification only, assigning each image to one of the predefined classes combining milk type and melamine level. The model was not designed to output continuous concentration values.

CNN optimization is generally carried out using entropic algorithms and a regularization method based on Semi-Global Matching to avoid overfitting, while maintaining high accuracy and fast computational speed (Izquierdo, Lastra-Mejías, González-Flores, Pradana-López, et al., 2020b). Within the parameter optimization, the learning phase of the mathematical algorithm is iterative, so it is very important to define the step size of each iteration. Moreover, this step is controlled by the learning coefficient, so the best coefficient value should be chosen to optimize all the parameters of the CNN and increase the generalization capability of the CNN (Pradana-López et al., 2022). It should be noted that the learning coefficient affects the rate of error reduction per iteration or epoch. Likewise, in order to reduce the computational power required to train this type of models, in this work, it has been necessary to reduce the number of images or batches used for the optimization of the model.

Residual neural networks (ResNet) are CNNs based on transfer learning, composed of a large number of computational layers that can vary, typically between 18 and 101. In this work, a ResNet34 is used to classify thermographic images of pure and adulterated powdered milk, which is a pre-trained network composed of 34 layers. This model is based on the transfer of the data of the first layers from one model to another. The first layers are frozen, while the final layers are optimized according to the specifications of the analysis to be performed (Pradana-López et al., 2021, 2022).

The total image dataset consisted of 28,485 frames, which were divided into three independent subsets: training (20,292 images), internal verification (5187 images), and blind validation (3006 images). These subsets were described in detail in Section 3.1. The training dataset is used to calculate errors and optimize the learning parameters or weights. After each iteration in training, the internal verification set is applied to avoid overlearning and ensure internal generalization. Finally, the blind validation images test the model and check whether it meets the desired specifications. The statistical performance of the CNN is quantified by the overall accuracy (correct classification rate) and the specific accuracy of correctly classified images of each individual class (Estrada-Pérez et al., 2021).

2.4. Thermographic image conditioning

The thermographic images were collected from the original videos in TIFF format, initially measuring 382 × 288 pixels. To reduce the computational load on the CNN algorithm, the frames were resized to 200 × 200 pixels. To ensure that the model focused on the thermographic profile rather than the sample shape, the images were then randomly cropped to 100 × 100 pixels. These cropped images served as the dataset for training and validating the ResNet34 model.

To maintain consistency and a broad window of operation in region selection, the image preprocessing stage involved a specific cropping and random sampling strategy. The region of interest (ROI) was automatically identified in each image, as the frames clearly distinguish between the relevant sample (milk powder) and the irrelevant background (see Fig. 1). From this ROI, multiple random patches of 100 × 100 pixels were extracted from different locations to capture varied thermal signatures. This ensured that the CNN training dataset contained a diverse set of representative examples from the sample region, enhancing the robustness and generalization capability of the model.

The complexity of distinguishing thermographic images is evident when comparing the images at a given average temperature, as they are very similar to the naked eye. Therefore, it is necessary to resort to algorithms like CNNs, which are able to identify patterns that relate the characteristics of an image within a group, with the objective of classifying the images qualitatively and quantitatively. The images of both pure samples (Fig. 1) and adulterated samples (Fig. 2) show that the distribution of colors in the heat map varies according to the type of milk and melamine concentration, which will help the CNNs classify the images correctly.

3. Results and discussion

In this section, the results derived from the optimized ResNet34 model to classify powdered milk samples based on their melamine content are presented and discussed.

3.1. ResNet34: optimization, verification, and blind testing

The large image database, consisting of 28,485 frames, was randomly separated into two main groups to properly train the ResNet34 model. It is essential for these groups to remain independent to prevent overfitting. Accordingly, ~10 % of the images (3,006) were initially isolated for blind validation. The remaining ~90 % (25,479 images) were further divided into ~80 % (20,292) for training and ~20 % (5187) for internal verification.

The thermographic dataset included 31 distinct classes, comprising three types of powdered milk (whole, skimmed, and infant), each adulterated with nine melamine concentrations (0.5–10 ppm), plus a non-adulterated control and a pure melamine sample. Each class contained approximately 360 frames, and from each frame, three random thermograms (or cropped thermal images) were initially extracted. However, some of these thermograms were identified as incorrect or defective and subsequently discarded, resulting in around 930 valid thermograms per class and a total of 28,485 thermograms. The dataset was relatively balanced across classes, with no substantial imbalance that required corrective weighting. Therefore, no class weighting or oversampling strategies were applied. Additionally, the random selection of image regions and large number of frames per sample contributed to maintaining representative variability within each class. The dataset was partitioned randomly into the three subsets mentioned above, ensuring proportional representation of all milk types and melamine concentrations within each subset. This preserved class balance and minimized selection bias throughout model development and evaluation. These classes were constructed from three independent physical replicates per concentration and milk type, ensuring that the thermal patterns learned by the model are not biased by single-sample artifacts.

The blind validation set, selected prior to any training or optimization, simulates the real-world deployment scenario in which the model is applied to previously unseen data. As such, it constitutes a true independent validation, providing a realistic and unbiased assessment of the model's generalization performance. Its early separation ensures that no data leakage occurred during model tuning, thereby reinforcing the methodological rigor and robustness of the final algorithm. While the class labels correspond to specific melamine concentration levels, the model operates strictly as a classifier. No attempt was made to interpolate or estimate concentration values between classes.

3.1.1. CNN training and internal verification

The main parameters of the implemented ResNet34 model used to optimize its weights and train the network are presented in Table 1.

Although the model achieved high accuracy, the training process was carefully optimized by selecting a low learning rate range ($2\cdot10^{-6}$ to $6\cdot10^{-4}$), a batch size of 64, and a limited number of epochs (3), which were sufficient to achieve convergence without overfitting. These hyperparameters were identified as the most appropriate to solve the specific classification problem addressed in this study, balancing computational efficiency with model performance and generalization capability.

After training the CNN, the network was internally verified to monitor the learning process and assess its ability to generalize beyond the training data. The confusion matrix obtained from the internal validation set is presented in Fig. 3a.

This matrix compares the actual melamine concentrations with the predictions made by the trained ResNet34 model. Classification was performed across 31 classes: four pure samples (three milk types and melamine) and 27 adulterated samples (nine melamine concentrations × three milk types). The internal validation accuracy was 98.54 %, with only 75 misclassifications out of 5187 images, confirming the high reliability and robustness of the proposed approach (Pradana-López et al., 2022).

Regarding individual predictions, the model was able to correctly identify the milk type in most cases, but occasionally misclassified the specific concentration of melamine. This suggests that thermographic profiles for the same milk type are very similar across adjacent concentration levels, with only subtle differences.

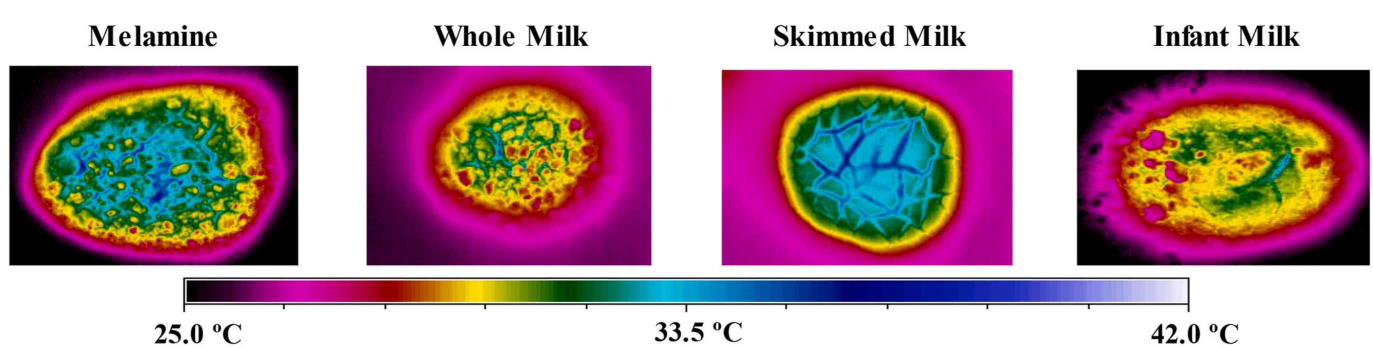

Fig. 1. Raw thermographic example frames (382 × 288 pixels) extracted at an average temperature of 38 °C for each type of pure product (powdered milk and melamine).

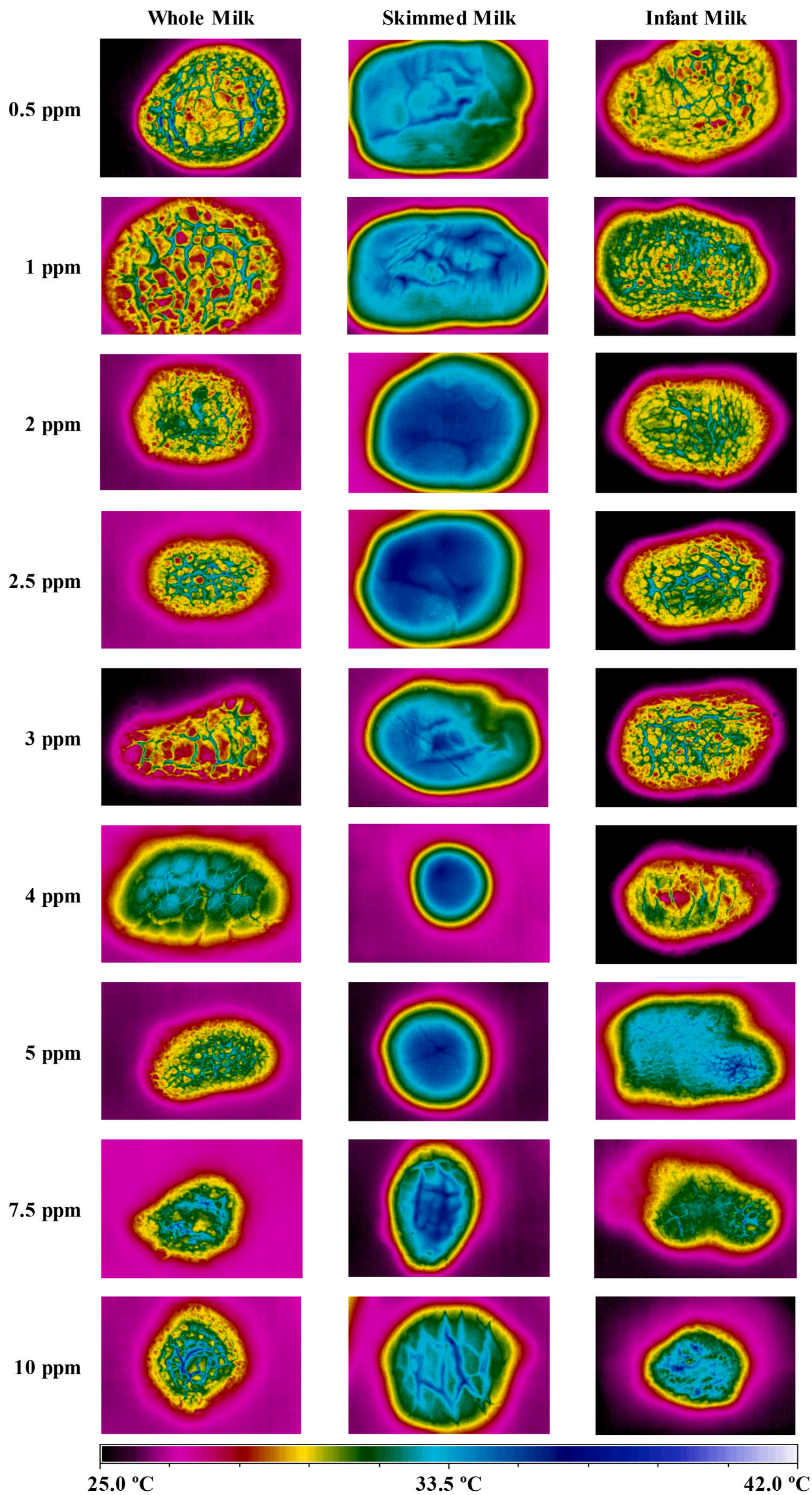

Fig. 2. Raw thermographic example frames (382 × 288 pixels) extracted at an average temperature of 38 °C for each type of powdered milk adulterated with melamine (ppm).

Table 1
Parameters of the ResNet34 model.

Parameters	
Range of learning coefficient	$2{\cdot}10^{-6}$ - $6{\cdot}10^{-4}$
Size of inputted images (vertical pixels × horizontal pixels × RGB channels)	100 × 100 × 3
Stride	1
Number of epochs	3
Mini-batch size	64

3.1.2. Testing with blinded images

Once the training and internal validation of the model was completed, the blind validation with 10 % of the images was performed. Of the 3006 images available, 2966 were correctly classified, leading to a total accuracy of 98.67 %. These results, together with those obtained in the internal verification, confirm the robustness of ResNet34 for detecting the type of milk powder and quantifying the melamine concentration within the low ppm scale, specifically in the range of 0.5–10 ppm. It should be noted that the melamine range analyzed encompasses concentrations lower than those legally accepted in milk powders, both for adults (2.5 ppm) and infants, which would be interpreted as "melamine-free" milk samples (Pradana-López et al., 2022).

The confusion matrix obtained from this process is presented in Fig. 3b. The incorrect results, along with their predicted classes, are shown in Table 2, while some of these misclassified images are displayed in Fig. 4.

It was observed that these cropped images are often black regions or lack significant features that could support accurate classification, typically corresponding to the edges of the original images (Fig. 4). In most misclassifications, the milk type was correctly identified, but not the melamine concentration. Conversely, cropped images rich in detail, color variation, and texture are rarely misclassified (Fig. 5), as they contain features that the model has learned to recognize during training.

This observation led to the implementation of a pre-filtering step based on image quality metrics such as thermal contrast, entropy, or edge detection. By removing images with low information content or minimal thermal variation, the model was trained and validated using only meaningful thermograms. As a result, the number of classification errors—particularly at low melamine concentrations—was reduced, enhancing both the discriminative power of the network and the generalizability of the results.

To estimate the detection capabilities of the proposed method, the classification accuracy for samples containing the lowest melamine concentration tested (0.5 ppm) was analyzed. Across the three milk types (whole, skimmed, and infant), the blind validation results showed classification accuracies of 100.0 %, 97.9 %, and 98.9 %, respectively. These results indicate that the model can reliably detect melamine adulteration at concentrations as low as 0.5 ppm, which is below the legal threshold for infant formula (1.0 ppm).

Given the classification-based nature of the method, the limit of detection (LOD) is defined empirically as the lowest concentration for which classification accuracy exceeds 95 %. According to this criterion, the LOD of the proposed CNN-based thermographic method is 0.5 ppm.

Although alternative approaches—such as estimating the LOD via the 3σ criterion using the standard deviation of the negative control (melamine-free samples)—are common in quantitative analytical chemistry, their direct application to classification models is limited. Therefore, a performance-based empirical LOD, validated through cross-validated blind testing, is considered more appropriate in this context.

In summary, powdered milk adulterated with melamine in the concentrations studied cannot be visually distinguished by the human eye. This reinforces the utility of thermographic imaging combined with CNNs as a reliable alternative for accurate detection. In fact, Pradana-López et al. (2022) achieved similar results in detecting melamine in the same three types of powdered milk (whole, skimmed, infant) using optical images and a ResNet34 model, with an overall classification accuracy of 97.0 %. These promising findings confirm that both thermographic and optical imaging, when paired with CNN-based deep learning algorithms, are valuable tools for identifying potential food fraud.

Interestingly, the higher misclassification rate observed for pure infant milk powder samples, compared to the adulterated ones, can be attributed to both physical and chemical factors. Physically, infant milk powder typically has a finer and more homogeneous particle structure, which can lead to thermal signatures during cooling that are more similar to those of other milk types, especially in the absence of melamine. Chemically, infant formulas contain various additives such as maltodextrins and vegetable oils to meet the nutritional needs of infants. These additives have been reported to modify the thermal conductivity and heat retention properties of the product, resulting in overlapping thermal responses between different pure milk samples (Saxena et al., 2021; Sun et al., 2018). This may explain the higher incidence of misclassification errors observed in the pure infant milk powder samples in this study, compared to other types of milk powder. In contrast, whole and skimmed milk powders have more consistent compositions and fewer additives, making the thermal profiles between pure and adulterated samples more distinguishable and thus reducing the likelihood of misclassification.

These classification results and accuracy metrics are consistent with recent studies that have employed advanced imaging and deep learning techniques for food fraud detection. For example, similar approaches have been used to detect different adulterants in cinnamon powder using hyperspectral imaging (Zhang et al., 2024), to identify fraud in black and red peppers (Li et al., 2024), and to assess fungal infection in pistachio kernels via thermal imaging (Kheiralipour et al., 2015). This consistency confirms that the proposed thermographic and deep learning-based method is robust and comparable to state-of-the-art methods in similar domains (Huerta-Herraiz et al., 2019; Pradana-López et al., 2022). Furthermore, the high classification accuracy suggests that the method can be integrated into rapid quality control workflows in dairy product processing plants, particularly for early detection and screening purposes.

This study has focused exclusively on the detection of melamine in powdered milk and did not include systematic testing with other nitrogen-containing compounds such as urea, creatinine, or ammonium sulfate, which could also affect the thermal profile. While this approach is justified by the proof-of-concept nature of the work, the results obtained validate the methodology and pave the way for future studies aimed at expanding the experimental scope through the inclusion of additional adulterants. This would make it possible to assess whether the thermographic patterns detected by the neural network are specific to melamine or represent a more general thermal response to the presence of nitrogen-rich compounds. This line of future research will be essential to reinforce the practical applicability of the method in real-world quality control scenarios.

3.2. Thermal features and their relationship with classification accuracy

A qualitative analysis of the thermographic images used in this study reveals an association between specific thermal patterns and the classification performance of the convolutional neural network. Although the images may appear visually similar at a glance, subtle differences in thermal structure—such as localized gradients, contour definition, and internal texture—vary consistently with both the type of milk and the melamine concentration.

In samples of whole milk adulterated with higher melamine concentrations, the thermal images typically display irregular temperature distributions, including sharp internal gradients and thermal "islands" that suggest altered heat transfer dynamics. In contrast, samples with low melamine concentrations tend to exhibit smoother, more homogeneous cooling patterns, Fig. 2. Infant milk powders, due to their finer

(a)	PREDICTED																													
ACTUAL	W	W-0.5	W-1	W-2	W-2.5	W-3	W-4	W-5	W-7.5	W-10	I	I-0.5	I-1	I-2	I-2.5	I-3	I-4	I-5	I-7.5	I-10	S	S-0.5	S-1	S-2	S-2.5	S-3	S-4	S-5	S-7.5	S-10
W	214	0	0	0	0	0	0	0	0	0	0	0	0	0	0	0	0	0	0	0	0	0	0	0	0	0	0	0	0	0
W-0.5	0	311	0	0	0	0	0	0	0	0	0	0	0	0	0	0	0	0	0	0	0	0	0	0	0	0	0	0	0	0
W-1	0	0	286	0	0	0	0	0	0	0	0	0	0	0	0	0	0	0	0	0	0	0	0	0	0	0	0	0	0	0
W-2	1	0	0	269	0	0	0	0	0	0	0	0	0	0	0	0	0	0	0	0	0	0	0	0	0	0	0	0	0	0
W-2.5	1	0	1	4	292	0	0	0	2	0	0	0	0	0	0	0	0	0	0	0	0	0	0	0	0	0	2	0	0	0
W-3	0	0	0	0	0	269	0	0	0	0	0	1	0	0	0	0	0	0	0	0	0	0	0	0	0	0	0	0	0	0
W-4	0	0	0	0	0	0	157	0	0	0	0	0	0	0	0	0	0	0	0	0	0	0	0	0	0	0	0	0	0	0
W-5	1	0	0	2	0	0	0	152	0	0	0	0	0	0	0	0	0	1	0	0	0	0	0	0	0	0	0	0	0	0
W-7.5	0	0	0	0	0	0	0	0	191	1	0	0	0	0	0	0	0	0	0	0	0	0	0	0	0	0	2	0	0	0
W-10	0	0	0	0	0	0	0	0	0	231	0	0	0	0	0	0	0	0	0	0	0	0	0	0	0	0	0	0	0	0
I	0	0	0	0	0	0	0	0	0	0	83	0	0	0	0	0	1	0	0	0	0	0	0	0	0	0	0	0	0	0
I-0.5	**3**	1	0	0	0	0	0	1	0	0	0	147	0	0	0	0	0	0	0	0	0	0	0	0	0	0	0	0	0	0
I-1	0	0	0	0	0	0	0	0	0	0	0	0	89	0	0	1	0	0	0	0	0	0	0	0	0	0	0	0	0	0
I-2	0	0	0	0	0	0	0	0	0	0	0	0	0	56	1	1	0	0	0	0	0	0	0	0	0	0	0	0	0	0
I-2.5	0	0	0	0	0	0	0	0	0	0	**5**	0	0	0	87	0	0	0	0	0	0	0	0	0	0	0	0	0	0	0
I-3	0	0	0	0	0	0	0	0	0	0	2	0	1	1	0	71	0	0	0	0	0	0	0	0	0	0	0	0	0	0
I-4	0	0	0	0	0	0	0	0	0	0	**16**	0	0	0	0	0	52	0	0	0	0	0	0	0	0	0	0	0	0	0
I-5	0	0	0	0	0	0	0	0	0	0	0	0	0	0	0	0	0	53	0	0	0	0	0	0	0	1	0	0	0	0
I-7.5	0	0	0	0	0	0	0	0	0	0	0	2	0	0	0	0	0	0	53	0	0	0	0	0	0	0	0	0	0	0
I-10	0	0	0	0	0	0	0	0	0	0	0	0	0	0	0	0	0	0	0	51	0	0	0	0	0	0	0	0	0	0
S	1	0	1	0	0	0	0	0	0	0	0	0	0	0	0	0	0	0	0	0	123	0	0	0	2	0	0	0	0	**4**
S-0.5	0	2	0	0	0	0	0	0	0	0	0	0	0	0	0	0	0	0	0	0	0	239	0	0	0	0	0	0	0	0
S-1	0	0	0	0	0	0	0	0	0	0	0	0	0	0	0	0	0	0	0	0	0	0	228	0	0	0	0	0	0	0
S-2	0	0	0	0	0	0	0	0	0	0	0	0	0	0	0	0	0	0	0	0	0	0	0	267	0	0	0	0	0	0
S-2.5	0	0	1	0	0	0	0	0	1	0	0	0	0	0	0	0	0	0	0	0	0	0	0	0	214	0	0	0	0	0
S-3	0	0	1	0	0	0	0	0	0	0	0	0	0	0	0	0	0	0	0	0	0	0	0	0	0	193	0	0	0	0
S-4	0	0	0	0	0	0	0	0	2	1	0	0	0	0	0	0	0	0	0	0	0	0	0	0	0	0	185	0	0	0
S-5	0	0	0	0	0	0	0	0	0	0	0	1	0	0	0	0	0	0	0	0	0	0	0	0	0	0	0	166	0	0
S-7.5	0	0	0	0	0	0	0	0	0	0	0	0	0	0	0	0	0	0	0	0	0	0	0	0	0	0	0	1	171	0
S-10	0	0	0	0	0	0	0	0	0	0	0	0	0	0	0	0	0	0	0	0	0	0	0	0	1	0	0	0	0	182

(b)	PREDICTED																													
ACTUAL	W	W-0.5	W-1	W-2	W-2.5	W-3	W-4	W-5	W-7.5	W-10	I	I-0.5	I-1	I-2	I-2.5	I-3	I-4	I-5	I-7.5	I-10	S	S-0.5	S-1	S-2	S-2.5	S-3	S-4	S-5	S-7.5	S-10
W	143	0	0	0	0	0	0	0	0	0	0	0	0	0	0	0	0	0	0	0	0	0	0	0	0	0	0	0	0	0
W-0.5	0	155	0	0	0	0	0	0	0	0	0	0	0	0	0	0	0	0	0	0	0	0	0	0	0	0	0	0	0	0
W-1	0	0	167	0	0	0	0	0	0	0	0	0	0	0	0	0	0	0	0	0	0	0	0	0	0	0	0	0	0	0
W-2	1	0	0	183	0	0	0	0	0	0	0	0	0	0	0	0	0	0	0	0	0	0	0	0	0	0	0	0	0	0
W-2.5	0	0	0	1	155	0	0	0	2	0	0	0	0	0	0	0	0	0	0	0	0	0	0	0	0	0	0	0	0	0
W-3	0	0	0	0	0	165	0	0	0	0	0	0	0	0	0	0	0	0	0	0	0	0	0	0	0	0	0	0	0	0
W-4	0	0	0	0	0	0	70	0	0	0	0	0	0	0	0	0	0	0	0	0	0	0	0	0	0	0	0	0	0	0
W-5	0	0	0	1	0	0	0	89	0	0	0	0	0	0	0	0	0	0	0	0	0	0	0	0	0	0	0	0	0	0
W-7.5	0	0	0	0	0	0	0	0	92	0	0	0	0	0	0	0	0	0	0	0	0	0	0	0	0	0	0	0	0	0
W-10	0	0	0	0	0	0	0	0	0	139	0	0	0	0	0	0	0	0	0	0	0	0	0	0	0	0	0	0	0	0
I	0	0	0	0	0	0	0	0	0	0	45	0	0	0	0	0	2	0	0	0	0	0	0	0	0	0	0	0	0	0
I-0.5	0	0	0	0	0	0	0	1	0	0	0	96	0	0	0	0	0	0	0	0	0	0	0	0	0	0	0	0	0	0
I-1	0	0	0	0	0	0	0	0	0	0	0	0	59	0	0	0	0	0	0	0	0	0	0	1	0	0	0	0	0	0
I-2	0	0	0	0	0	0	0	0	0	0	0	0	0	54	0	0	0	0	0	0	0	0	0	0	0	0	0	0	0	0
I-2.5	0	0	0	0	0	0	0	0	0	0	1	0	0	0	43	0	0	0	0	0	0	0	0	0	0	0	0	0	0	0
I-3	0	0	0	0	0	0	0	0	0	0	1	0	0	1	0	45	0	0	0	0	0	0	0	0	0	0	0	0	0	0
I-4	0	0	0	0	0	0	0	0	0	0	**14**	0	0	0	0	0	35	0	0	0	0	0	0	0	0	0	0	0	0	0
I-5	0	0	1	0	0	0	0	0	0	0	0	0	0	0	0	0	0	28	0	0	0	0	0	0	0	0	0	0	0	0
I-7.5	0	0	0	0	0	0	0	0	0	0	0	0	0	0	0	0	0	0	30	0	0	0	0	0	0	0	0	0	0	0
I-10	0	0	0	0	0	0	0	0	0	0	0	0	0	0	0	0	0	0	0	44	0	0	0	0	0	0	0	0	0	0
S	0	0	0	0	0	0	0	0	0	0	0	0	0	0	0	0	0	0	0	0	70	0	0	0	0	0	1	0	0	0
S-0.5	0	1	0	0	0	0	0	0	0	0	0	0	0	0	0	0	0	0	0	0	1	120	0	0	0	0	0	0	0	0
S-1	0	0	0	0	0	0	0	0	0	0	0	0	0	0	0	0	0	0	0	0	0	0	132	0	0	0	0	0	0	0
S-2	0	0	0	0	0	0	0	0	0	0	0	0	0	0	0	0	0	0	0	0	0	0	0	163	0	0	0	0	0	0
S-2.5	0	0	0	0	0	0	0	0	0	0	0	0	0	0	0	0	0	0	0	0	1	0	0	0	99	0	0	0	0	0
S-3	0	0	2	0	0	0	0	0	0	0	0	0	0	0	0	0	0	0	0	0	0	0	0	0	0	129	0	0	0	0
S-4	0	0	0	0	0	0	0	0	**4**	1	0	0	0	0	0	0	0	0	0	0	0	0	0	0	0	1	109	0	0	0
S-5	0	0	0	0	0	0	0	0	0	0	0	0	0	0	0	0	0	0	0	0	0	0	0	0	0	0	0	110	0	0
S-7.5	0	0	0	0	0	1	0	0	0	1	0	0	0	0	0	0	0	0	0	0	0	0	0	0	0	0	0	1	98	0
S-10	0	0	0	0	0	0	0	0	0	0	0	0	0	0	0	0	0	0	0	0	0	0	0	0	0	0	0	0	0	99

Fig. 3. Confusion matrices for the optimized model: (a) internal validation and (b) blind validation with independent images.

Table 2
Incorrectly classified images during blind validation of the developed model.

Real label (product, melamine concentration)	Number of misclassifications	Predicted label (product, melamine concentration)
Whole, 2 ppm	1	Whole
Whole, 2.5 ppm	1	Whole, 2 ppm
Whole, 5 ppm	1	Whole, 2 ppm
Infant	2	Infant, 4 ppm (x2)
Infant, 0.5 ppm	1	Whole, 5 ppm
Infant, 1 ppm	1	Infant, 2 ppm
Infant, 2.5 ppm	1	Infant
Infant, 3 ppm	2	Infant; Infant, 2 ppm
Infant, 4 ppm	14	Infant (x14)
Infant, 5 ppm	1	Whole, 1 ppm
Skimmed	1	Skimmed, 4 ppm
Skimmed, 0.5 ppm	2	Skimmed; Whole, 0.5 ppm
Skimmed, 2.5 ppm	1	Skimmed
Skimmed, 3 ppm	2	Skimmed, 1 ppm (x2)
Skimmed, 4 ppm	6	Skimmed, 2.5 ppm; Whole, 10 ppm; Whole, 7.5 ppm (x4)
Skimmed, 7.5 ppm	3	Skimmed, 5 ppm; Whole, 10 ppm; Whole, 3 ppm

particle structure and lower fat content, often present well-defined radial symmetry in the thermal profiles, especially at low adulteration levels.

These thermographic characteristics influence the classification output of the model. Images containing rich thermal features—such as structured variation in the core region or distinct boundaries between temperature zones—are more reliably classified into their correct categories. On the other hand, images with poor thermal contrast or lacking internal complexity are more frequently associated with misclassifications Fig. 4. This suggests that the model effectively learns and exploits patterns that are physically meaningful, rather than relying on spurious or incidental visual traits.

The importance of image content and thermophysical variability has been highlighted in other studies using imaging techniques for food quality control (Gowen et al., 2010), where minor structural or compositional changes lead to discernible patterns in thermal or optical signals. The findings of the present study align with this evidence, demonstrating that accurate detection of food adulteration using thermographic imaging depends not only on the analytical model but also on the presence of thermally informative structures in the image data.

4. Conclusions

In this study, a deep learning-based analysis of thermographic images using a ResNet34 convolutional neural network was successfully applied to detect melamine adulteration categorically in three types of powdered milk. The optimized ResNet34 model achieved an overall classification accuracy of 98.67 % and a detection limit of 0.5 ppm, which is sufficiently sensitive to identify adulteration below the legal thresholds.

These results confirm that the ResNet34 architecture is highly sensitive to subtle thermal differences in milk powders adulterated with melamine, learning meaningful thermal patterns associated with milk type and melamine concentration. This study demonstrates that thermographic imaging, combined with deep learning, is a reliable, non-destructive, and rapid alternative to more complex analytical methods, offering a practical solution for the detection of melamine in powdered milk, particularly useful for high-throughput quality control applications or on-site evaluations. Furthermore, although this work represents a proof-of-concept focused exclusively on melamine detection, future studies should investigate the selectivity of the method against other potential adulterants to validate its applicability in more complex food fraud scenarios.

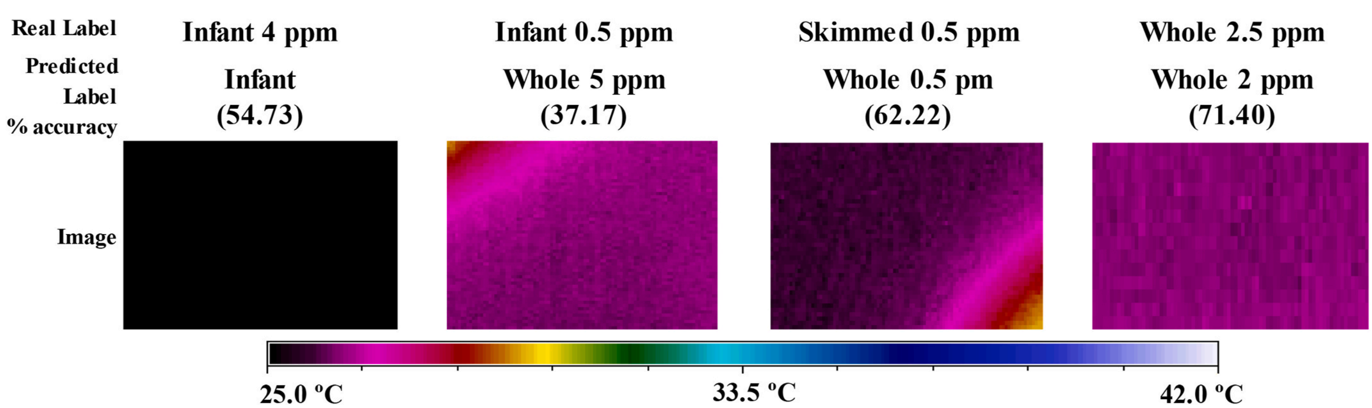

Fig. 4. Examples of images incorrectly classified during blind validation.

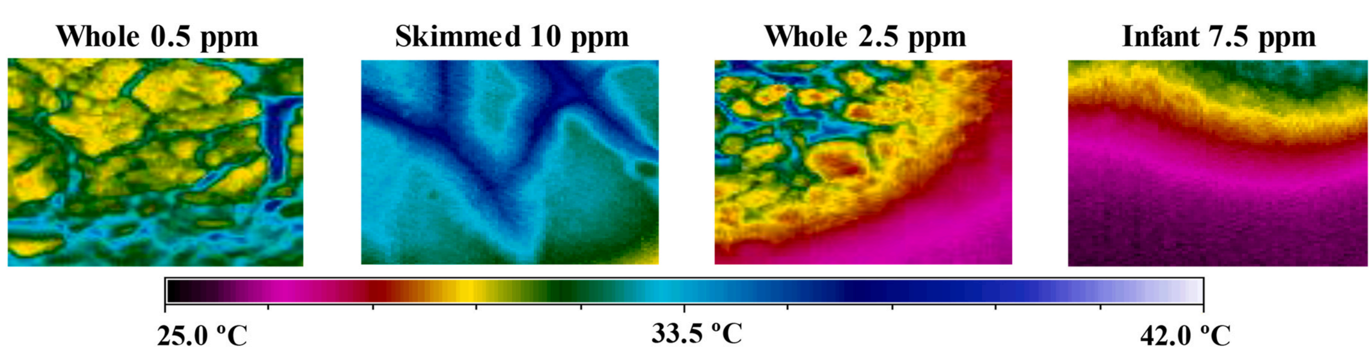

Fig. 5. Examples of images correctly classified during blind validation.

CRediT authorship contribution statement

Alicia Ortiz-Chiliquinga: Writing – original draft, Supervision, Software, Methodology, Investigation, Formal analysis, Conceptualization. **Ana M. Pérez-Calabuig:** Writing – original draft, Visualization, Validation, Supervision, Software, Methodology, Investigation, Data curation, Conceptualization. **Sandra Pradana-López:** Writing – original draft, Visualization, Validation, Supervision, Software, Methodology, Investigation, Formal analysis, Data curation, Conceptualization. **John C. Cancilla:** Writing – review & editing, Writing – original draft, Validation, Investigation, Conceptualization. **José S. Torrecilla:** Writing – review & editing, Writing – original draft, Visualization, Validation, Supervision, Software, Resources, Project administration, Methodology, Investigation, Funding acquisition, Formal analysis, Data curation, Conceptualization.

Declaration of competing interest

The authors declare that they have no known competing financial interests or personal relationships that could have appeared to influence the work reported in this paper.

Acknowledgments

This work has been partially funded by the FEI program of the Complutense University of Madrid under the project reference FEI-EU-17-03 and FEI 18/10.

Data availability

Data will be made available on request.

References

Bernabe, S., González, C., Fernández, A., & Bhangale, U. (2021). Portability and acceleration of deep learning inferences to detect rapid earthquake damage from VHR remote sensing images using intel OpenVINO toolkit. *Ieee Journal of Selected Topics in Applied Earth Observations and Remote Sensing, 14*, 6906–6915. https://doi.org/10.1109/JSTARS.2021.3075961

Cancilla, J. C., Pradana-López, S., Pérez-Calabuig, A. M., López-Ortega, S., Rodrigo, C., & Torrecilla, J. S. (2022). Distinct thermal patterns to detect and quantify trace levels of wheat flour mixed into ground chickpeas. *Food Chemistry, 384*, Article 132468. https://doi.org/10.1016/j.foodchem.2022.132468

Chandan, R. C., & Kilara, A. (2011). *Dairy ingredients for food processing*. Wiley-Blackwell.

Estrada-Pérez, L. V., Pradana-López, S., Pérez-Calabuig, A. M., Mena, M. L., Cancilla, J. C., & Torrecilla, J. S. (2021). Thermal imaging of rice grains and glours to design convolutional systems to ensure quality and safety. *Food Control, 121*, Article 107572. https://doi.org/10.1016/j.foodcont.2020.107572

European Union. (2008). Decisión de la Comisión de 14 octubre de 2008, por la que se establecen las condiciones particulares de importación de productos que contienen leche o productos lácteos originarios o procedentes de China, y se deroga la Decisión 2008/757/CE de la Comisión. *Diario Oficial Unión Europea, L273/19*, 18–20.

Feng, W., Lv, C., Yang, L., Cheng, J., & Yan, C. (2012). Determination of melamine concentrations in dairy samples. *LWT - Food Science and Technology, 47*(1), 147–153. https://doi.org/10.1016/j.lwt.2011.12.021

Finete, V. L., Gouvea, M., Marques, F., & Netto, A. (2013). Is it possible to detect adulteration of milk or whey protein with melamine, urea and ammonium sulfate, combining kjeldahl and classical spectrophotometric methods? *Food Chemistry, 141*(4), 3649–3655. https://doi.org/10.1016/j.foodchem.2013.06.046

Gowen, A. A., Tiwari, B. K., McDonnell, K., & O'Donell, C. P. (2010). Applications of thermal imaging in food quality and safety assessment. *Trends in Food Science and Technology, 21*(4), 190–200. https://doi.org/10.1016/j.tifs.2009.12.002

Guo, H., Zhou, X., Zhang, Y., Song, B., Liu, L., Zhang, J., & Shi, H. (2014). Highly sensitive and rapid detection of melamine in milk products by planar waveguide fluorescence immunosensor. *Sensors and Actuators B Chemical, 194*, 114–119. https://doi.org/10.1016/j.snb.2013.12.058

Huerta-Herraiz, A., Pliego-Marugán, A., & García-Márquez, F. P. (2019). A review on condition monitoring system for solar plants based on thermography. In M. Papaelias, F. P. García Márquez, & A. Karyotakis (Eds.), *Non-destructive testing and condition monitoring techniques for renewable energy industrial assets* (pp. 103–118). Elsevier Inc.. https://doi.org/10.1016/B978-0-08-101094-5.00007-1. ISBN 978-0-12-809747-2.

Izquierdo, M., Lastra-Mejías, M., González-Flores, E., Cancilla, J. C., Pérez, M., & Torrecilla, J. S. (2020a). Convolutional decoding of thermographic images to locate and quantify honey adulterations. *Talanta, 209*, Article 120500. https://doi.org/10.1016/j.talanta.2019.120500

Izquierdo, M., Lastra-Mejías, M., González-Flores, E., Pradana-López, S., Cancilla, J. C., & Torrecilla, J. S. (2020b). Visible imaging to convolutionally discern and authenticate varieties of rice and their derived flours. *Food Control, 110*, Article 106971. https://doi.org/10.1016/j.foodcont.2019.106971

Kheiralipour, K., Ahmadi, H., Rajabipour, A., Rafiee, S., & Javan-Nikkhah, M. (2015). Classifying healthy and fungal infected-pistachio kernel by thermal imaging technology. *International Journal of Food Properties, 18*(1), 93–99. https://doi.org/10.1080/10942912.2012.717155

Lam, H. S., Pak, C. N., Chu, W. C., Wong, W., Chan, D. F., Ho, S. S., Wong, K. T., Ahuja, A. T., & Li, C. K. (2008). Renal screening in children after exposure to low dose melamine in Hong Kong: Cross sectional study. *British Medical Journal, 337*, 2991. https://doi.org/10.1136/bmj.a2991

Li, H., Chen, Y., Zhang, Q., Wang, L., Zhao, X., & Liu, Y. (2024). Visible feature engineering to detect fraud in black and red peppers. *Scientific Reports, 14*, Article 76617. https://doi.org/10.1038/s41598-024-76617-1

Liu, Y., Todd, E., Zhang, Q., Shi, J. R., & Liu, X. J. (2012). Recent developments in the detection of melamine. *Journal of Zhejiang University - Science B, 13*(7), 525–532. https://doi.org/10.1631/jzus.B1100389

Liu, Y., & Xu, L. (2023). Layer-by-Layer assembly of two-dimensional monolayer films of gold nanoparticles for electrochemical determination of melamine. *Analytical Letters, 56*(15), 2426–2442. https://doi.org/10.1080/00032719.2023.2174132

Pradana-López, S., Pérez-Calabuig, A. M., Cancilla, J. C., Lozano, M. A., Rodrigo, C., Mena, M. L., & Torrecilla, J. S. (2021). Deep transfer learning to verify quality and safety of ground coffee. *Food Control, 122*, Article 107801. https://doi.org/10.1016/j.foodcont.2020.107801

Pradana-López, S., Pérez-Calabuig, A. M., Cancilla, J. C., Otero, L., & Torrecilla, J. S. (2022). Single-digit ppm quantification of melamine in powdered milk driven by computer vision. *Food Control, 131*, Article 108424. https://doi.org/10.1016/j.foodcont.2021.108424

Ranjbar, S., Moghadas-Nejad, F., Zakeri, H., & Gandomi, A. H. (2020). Chapter 3 - Computational intelligence for modeling of asphalt pavement surface distress. In P. Samui, D. Kim, N. R. Iyer, & S. Chaudhary (Eds.), *New materials in civil engineering (79-116)*. Elsevier Inc.. https://doi.org/10.1016/B978-0-12-818961-0.00003-X. ISBN 978-0-12-818961-0.

Sánchez-Martín, A., Pellón-Olmedo, M., San Miguel-Hernández, A., Rodríguez-Barbero, E., & Pachón, J. (2018). Adulteración de Leches Infantiles con Melamina en China. *Gaceta Medica Bilbao: Revista Oficial de la Academia de Ciencias Médicas de Bilbao, 115*(3), 123–131.

Saxena, J., Adhikari, B., Brkljaca, R., Huppertz, T., Zisu, B., & Chandrapala, J. (2021). Influence of lactose on the physicochemical properties and stability of infant formula powders: A review. *Food Reviews International*. https://doi.org/10.1080/87559129.2021.1928182

Shalileh, F., Sabahi, H., Golbashy, M., Dadmehr, M., & Hosseini, M. (2023a). A simple smartphone-assisted paper-based colorimetric biosensor for the detection of urea adulteration in milk based on an environment-friendly pH-sensitive nanocomposite. *Analytica Chimica Acta, 1234*, Article 341935. https://doi.org/10.1016/j.aca.2023.341935

Shalileh, F., Sabahi, H., Golbashy, M., Dadmehr, M., & Hosseini, M. (2023b). Recent developments in DNA nanostructure-based biosensors for the detection of melamine adulteration in milk. *Microchemical Journal, 195*, Article 109316. https://doi.org/10.1016/j.microc.2023.109316, 2023.

Soffer, S., Ben-Cohen, A., Shimon, O., Amitai, M. M., Greenspan, H., & Klang, E. (2019). Convolutional neural networks for radiologic images: A radiologist's guide. *Radioloy, 290*(3), 590–606. https://doi.org/10.1148/radiol.2018180547

Spink, J., & Moyer, D. C. (2011). Defining the public health threat of food fraud. *Journal of Food Science, 76*(9), 156–163. https://doi.org/10.1111/j.1750-3841.2011.02417.x

Sun, X., Wang, C., Wang, H., & Guo, M. (2018). Effects of processing on structure and thermal properties of powdered preterm infant formula. *Journal of Food Science, 83*(6), 1685–1694. https://doi.org/10.1111/1750-3841.14162

Ting, F. F., Tan, Y. J., & Sim, K. S. (2019). Convolutional neural network improvement for breast cancer classification. *Expert Systems with Applications, 120*, 103–115. https://doi.org/10.1016/j.eswa.2018.11.008

Tittlemier, S. A. (2010). Methods for the analysis of melamine and related compounds in foods: A review. *Food Additives & Contaminants: Part A, 27*(2), 129–145. https://doi.org/10.1080/19440040903289720

Torrecilla, J. S., Aragón, J. M., & Palancar, M. C. (2008). Optimization of an artificial neural network by selecting the training function. application to olive oil mills waste. *Industrial & Engineering Chemistry Research, 47*(18), 7072–7080. https://doi.org/10.1021/ie8001205

Torrecilla, J. S., Mena, M. L., Yàñez-Sedeño, P., & García, J. (2007). Quantification of phenolic compounds in olive oil mill wastewater by artificial neural network/laccase biosensor. *Journal of Agricultural and Food Chemistry, 55*(18), 7418–7426. https://doi.org/10.1021/jf0703351

Wu, L., Zhang, Y., Chen, X., Li, Z., Huang, J., & Wang, Q. (2023). Feasibility study of detecting some milk adulterations using a LED-based Vis-SWNIR photoacoustic spectroscopy system. *Food Chemistry*. , Article 136411.. https://doi.org/10.1016/j.foodchem.2023.136411

Xie, W., Huang, Y., Yun, W., Tang, D., Zhang, H., Du, C., Zhu, Y., & Zhang, W. (2015). Simple pretreatment and portable UV-VIS spectrum instrument for the rapid detection of melamine in milk products. *Journal of Food Quality, 38*, 297–304. https://doi.org/10.1111/jfq.12146

Yamashita, R., Nishio, M., & Do, R. K. G. (2018). Convolutional neural networks: An overview and application in radiology. *Insights into Imaging, 9*, 611–629. https://doi.org/10.1007/s13244-018-0639-9

Yan, Y. (2012). Food safety and social risk in contemporary China. *Journal of Asian Studies, 71*(3), 705–729.

Yang, L., Wang, Y., Chen, D., & Liu, J. (2023). Rapid detection of melamine in milk using portable raman spectroscopy combined with chemometric analysis. *Spectrochimica Acta Part A: Molecular and Biomolecular Spectroscopy, 293*, Article 123143. https://doi.org/10.1016/j.saa.2023.123143

Zhang, Y. D., Pan, C., Sun, J., & Tang, C. (2018). Multiple sclerosis identification by convolutional neural network with dropout and parametric ReLU. *Journal of Computational Science, 28*, 1–10. https://doi.org/10.1016/j.jocs.2018.07.003

Zhang, Y., Wang, X., Liu, H., Chen, L., Li, M., & Zhao, J. (2024). Detection of different adulteration in cinnamon powder using hyperspectral imaging and artificial neural network method. *Results in Chemistry*. , Article 101644. https://doi.org/10.1016/j.rechem.2024.101644

Zhou, H., Jin, Y., Dai, L., Zhang, M., Qiu, Y., & Zheng, J. (2020). Differential diagnosis of benign and malignant thyroid nodules using deep learning radiomics of thyroid ultrasound images. *European Journal of Radiology, 127*, Article 108992. https://doi.org/10.1016/j.ejrad.2020.108992

Zhu, W., Ma, Y., Zhou, Y., & Romagnoli, J. (2018). Deep learning based soft sensor and its application on a pyrolysis reactor for compositions predictions of gas phase components. *Computer Aided Chemical Engineering, 44*, 2245–2250. https://doi.org/10.1016/B978-0-444-64241-7.50369-4

Zhu, R., Tu, X., & Huang, J. X. (2020). Chapter 7 - Deep learning on information retrieval and its applications. In H. Das, C. Pradhan, & N. Dey (Eds.), *Deep learning for data analytics foundations, biomedical applications and challenges* (pp. 125–153). Academic Press. https://doi.org/10.1016/B978-0-12-819764-6.00008-9. ISBN 978-0-1281-9764-6.